JBIS, Vol. 53, pp.74-78, 2000

Overview of Radiation Belt Modelling

D. HEYNDERICKX
Belgisch Instituut voor Ruimte-Aëronomie, Ringlaan 3, B-1180 Brussel, Belgium.

The Earth's trapped radiation belts were discovered at the beginning of the space age and were immediately recognised as a considerable hazard to space missions. Consequently, considerable effort was invested in building models of the trapped proton and electron populations, culminating in the NASA AP-8 and AE-8 models which have been the de facto standards since the seventies. The CRRES mission has demonstatred that the trapped radiation environment is much more complex than the static environment described by the old models. Spatial and especially temporal variations were shown to be much more important than previously thought, and to require more complex models than those in use at that time. Such models are now becoming available, but they are limited in spatial or temporal coverage, and no global, dynamic, trapped radiation belt model is forthcoming. It is therefore vital to co-ordinate future modelling efforts in order to develop new standard models.

1. Introduction

This paper presents a brief review of the main characteristics of the Earth's trapped radiation belts and of the engineering models that are used to evaluate mission fluxes and doses. More detailed descriptions of the Earth's radiation environment and the related physical processes can be found in references [1,2,3].

The Belgisch Instituut voor Ruimte-Aëronomie (BIRA) has developed for the European Space Agency (ESA) a World-Wide Web interface to models of the space environment and its effects on spacecraft and systems. The SPace ENVironment Information System (SPENVIS) can be accessed at http://www.spenvis.oma.be/spenvis. The figures in this paper, except those with a reference number, were produced with the SPENVIS plotting facilities.

2. The Earth's Trapped Radiation Environment

2.1 The Concept of Trapped Radiation

The motions of charged particles entering the magnetosphere from the solar wind and undergoing acceleration, or resulting from the decay of neutrons produced by cosmic ray interactions with the neutral atmosphere, are dominated by the magnetospheric magnetic field. The motion of these energetic charged particles consists of three components:

a) gyration about magnetic field lines;

b) movement of the gyration centre up and down magnetic field lines (guiding centre motion);

c) slow longitudinal drift of the guiding centre path around the Earth, westward for ions and eastward for electrons.

The resulting trajectories lie on toroidal surfaces, called drift shells, centred on the Earth's dipole centre. Particles confined to a drift shell can remain there for long periods, up to years for protons at altitudes of a few thousand kilometers, whence the term "trapped particles".

The population of charged particles stably trapped by the Earth's magnetic field consists mainly of protons with energies between 100 keV and several hundred MeV and electrons with energies between a few tens of keV and 10 MeV. There is also evidence for the existence of a narrow region centred around altitudes of about one Earth radius containing trapped heavy ions which are believed to be decelerated anomalous cosmic ray ions; the intensities of these heavy ions are several orders of magnitude below the intensities of trapped energetic protons in this region.

2.2 The Trapped Proton Population

The energetic (above 10 MeV) trapped proton population is confined to altitudes below 20,000 km, while lower energy protons cover a wider region, with

Based on a presentation at the Symposium "Space Hazards" sponsored by BNSC and DERA in collaboration with the BIS on 21-22 October 1998.

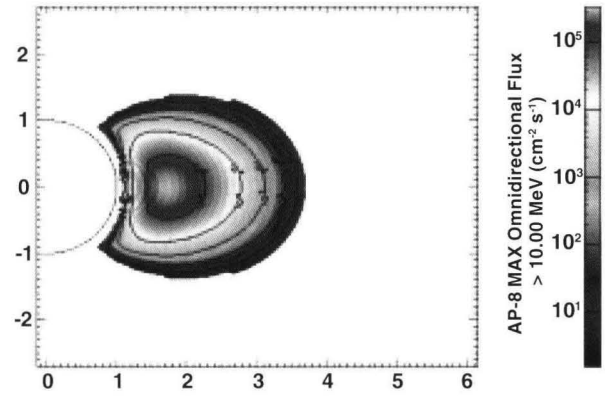

Fig. 1 Invariant coordinate map of the AP-8 MAX integral proton flux >10 MeV. The semi-circle represents the surface of the Earth, distances are expressed in Earth radii.

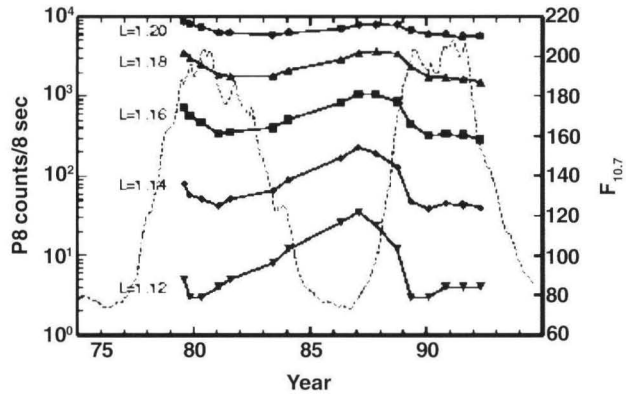

Fig. 3 Variation of proton count rates in the 80-215 MeV channel of the MEPED detector aboard the TIROS/NOAA spacecraft over the solar cycle as a function of *L* (7). The dashed line shows the 13-month smoothed solar $F_{10.7}$ flux.

protons below 1 MeV reaching geosynchronous altitudes. Figure 1 shows the distribution of trapped protons with energies above 10 MeV, as predicted by the NASA AP-8 MAX model [4], in invariant coordinate space. The region of space covered by higher energy protons diminishes with increasing energies and the location of the highest intensities moves inward.

2.3 The Trapped Electron Population

Figure 2 shows the AE-8 MAX [5] trapped electron population above 1 MeV in invariant coordinate space. The population distribution is characterised by two zones of high intensities, below altitudes of one Earth radius and above two Earth radii in the magnetic equatorial plane, respectively, which are separated by a region of low intensities, called the slot region. The location and extent of the inner and outer belts and of the slot region depends on electron energy, with higher energy electrons confined more to the inner belt, and lower energy electrons populating the outer belt to altitudes beyond geosynchronous orbit. Note that at high latitudes the outer electron belt reaches down to very low altitudes.

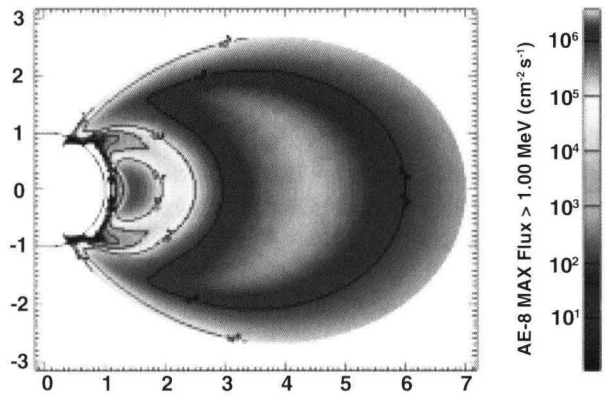

Fig. 2 Invariant coordinate map (see Fig. 1) of the AE-8 MAX integral electron flux >1 MeV.

2.4 Dynamics of the Trapped Particle Population

The general description of the radiation belts in Sections 2.2 and 2.3 represents what could be called the average particle distributions based on the static NASA models AP-8 and AE-8 [6]. However, it has long been established that the actual population is very dynamic over different time scales.

2.4.1 Solar Cycle Effects

The variation of solar irradiance with the 11-year solar cycle induces a periodicity of the low altitude trapped proton and electron fluxes: during solar maximum the Earth's neutral atmosphere expands compared to solar minimum conditions, so that the low altitude edges of the radiation belts are eroded due to increased interactions with neutral constituents. Figure 3 shows the variation of the low altitude trapped proton flux over the solar cycle [7]. The erosion effect increases with decreasing altitude and the recovery of the population shows a phase lag which also depends on altitude.

2.4.2 Secular Changes in the Geomagnetic Field

The low altitude trapped particle population is also influenced by secular changes in the geomagnetic field [8]: the location of the centre of the geomagnetic dipole field drifts away from the centre of the Earth at a rate of about 2.5 km/year (the separation currently exceeds 500 km), and the magnetic moment decreases with time. The combined effect is a slow inward drift of the innermost regions of the radiation belts.

The separation of the dipole centre from the

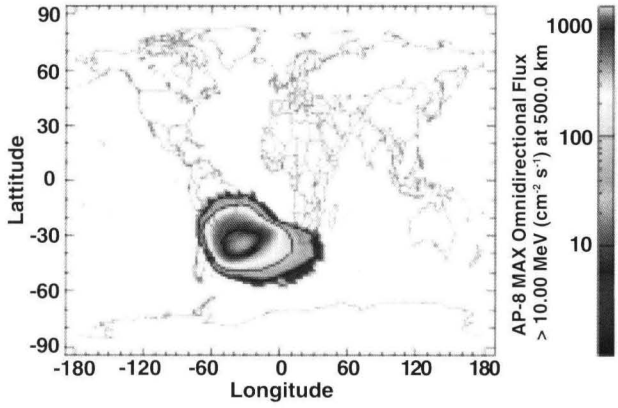

Fig. 4 World map of the AP-8 MAX integral proton flux >10 MeV at 500 km altitude.

Earth's centre and the inclination of the magnetic axis with respect to the rotation axis produce a local depression in the low altitude magnetic field distribution at constant altitude. As the trapped particle population is tied to the magnetic field, the lowest altitude radiation environment (below about 1,000 km) peaks in the region where the magnetic field is depressed [1]. This region is located to the south east of Brasil, and is called the South Atlantic Anomaly (SAA). Figures 4 and 5 represent a world map at 500 km altitude of the trapped proton (>10 MeV) and trapped electron (>1 MeV) distributions, respectively. The SAA shows up clearly in both maps. Proton fluxes are negligible outside the SAA, but electron fluxes can be very high at high latitudes where field lines from the outer electron belt reach down to low altitudes. A further effect of the secular change in the geomagnetic field is a slow westward drift of the SAA at a rate of 0.3 deg/year [9].

2.4.3 *Low Altitude Trapped Proton Anisotropy*

At low altitudes (typically below 2,000 km), trapped particles interact with the neutral atmosphere. The gyroradii of trapped protons with energies above 1 MeV are comparable to the atmospheric scale height, which means that during a gyration motion they encounter different atmospheric densities. As a result, proton fluxes depend on their arrival direction in the plane perpendicular to the local magnetic field vector (as well as on their pitch angle). The resulting anisotropy is called the East-West effect, and can cause differences of a factor three or more in fluxes arriving from different azimuths. The effect is illustrated in fig. 6, which shows the angular dependence of the AP-8 MAX integral proton flux >10 MeV, averaged over an 800 km heliosynchronous orbit.

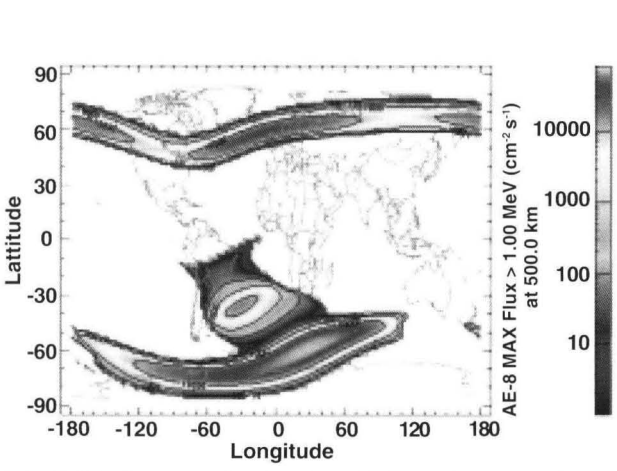

Fig. 5 World map of the AE-8 MAX integral electron flux >1 MeV at 500 km altitude.

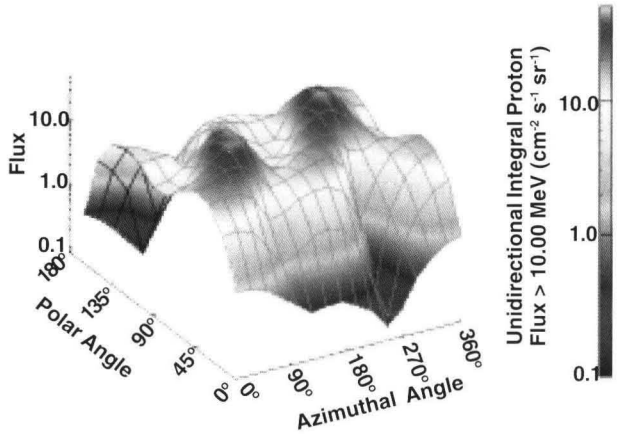

Fig. 6 Angular dependence of the AP-8 MAX integral proton flux >10 MeV, averaged over an 800 km heliosynchronous orbit. Angles are measured in a reference frame with its polar axis parallel to the satellite velocity vector.

2.4.4 *Magnetospheric Conditions*

Besides the long term variations in the trapped particle population described in Sections 2.4.1-2.4.2, variations on much shorter time scales occur as well. Outer zone electrons can vary in intensity by orders of magnitude over periods of a few hours. Measurements with instruments on board the Combined Release and Radiation Effects Satellite (CRRES) have shown that there are also major changes in the spatial distributions of outer zone electrons [10]. Gussenhoven et al. [11] have shown that the changes in flux and spatial distribution can be ordered by level of magnetospheric activity, i.e. the fifteen day running average of Ap. Figure 7 shows omnidirectional electron flux profiles on the magnetic equator as a function of McIlwain's L [12] for six ranges of Ap15.

CRRES Data also demonstrated that magnetic storms can greatly influence the trapped proton population [13]. The March 1991 storm created a second, stable high energy belt above L=1.8, with peak flux values exceeding pre-storm values by an

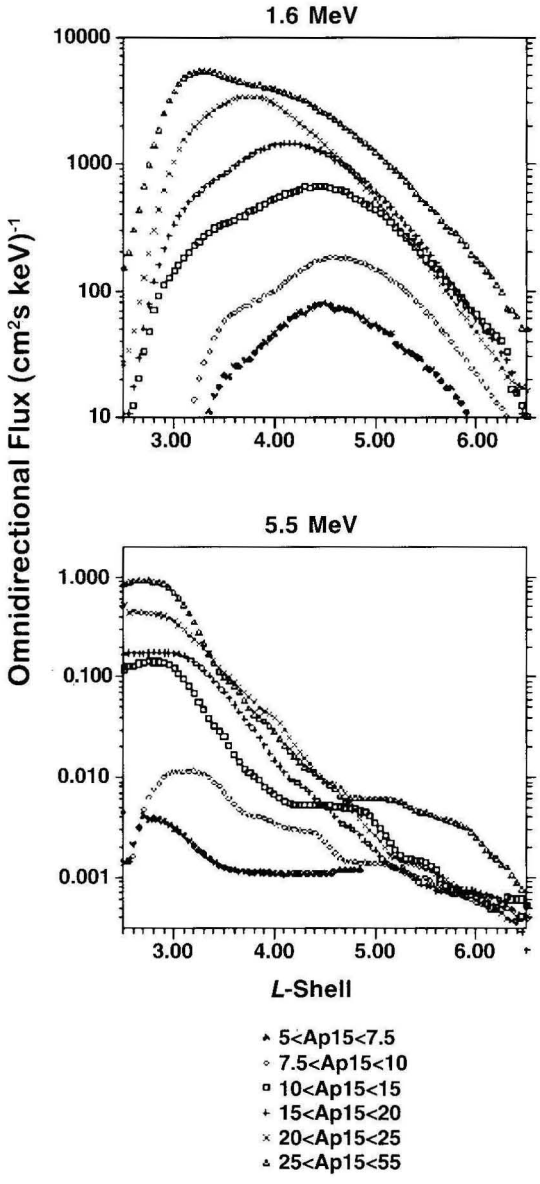

Fig. 7 Profiles of 1.6 MeV (top) and 5.5 MeV (bottom) omnidirectional electron flux on the magnetic equator, as a function of *L*, taken from the CRRES electron models for six ranges of Ap15 [11].

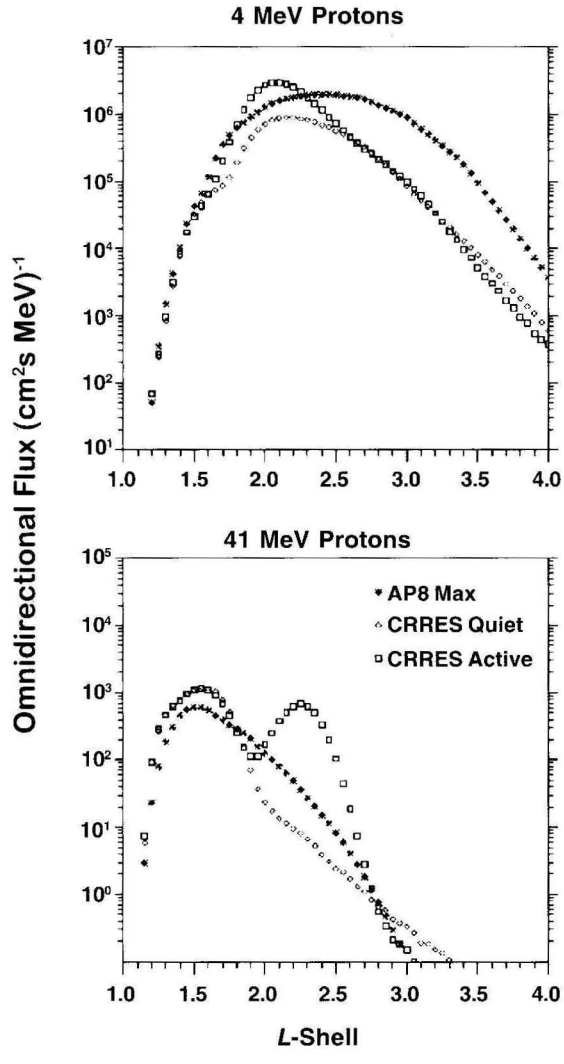

Fig. 8 Profiles of 4 MeV (top) and 41 MeV (bottom) omnidirectional proton flux on the magnetic equator, as a function of *L*, obtained with the CRRES quiet and active proton models and with AP-8 MAX [11].

order of magnitude [11], as shown in fig. 8. The newly-created proton belt decayed only very slowly and was still present six months later when the CRRES satellite was lost.

3. Effects of Trapped Radiation on Spacecraft and Components

Due to their large energy coverage, trapped particles cause a variety of effects in spacecraft, components and biological systems.

Low energy electrons contribute to spacecraft surface charging. High energy electrons injected and accelerated through the magnetotail can cause dielectric charge buildup deep inside geosynchronous spacecraft which may lead in turn to destructive arcing. Inner and outer belt electrons also contribute to ionising doses through direct energy deposition and bremsstrahlung effects.

High energy protons in the inner radiation belt are the main contributors to ionising dose deposition in shielded components. They also dominate Single Event Upset (SEU) rates at low altitudes and latitudes, where cosmic rays and solar energetic particles are effectively shielded by the geomagnetic field. Lower energy protons (up to 10 MeV) contribute to Non-Ionising Energy Loss (NIEL) dose which affects Charged-Coupled Devices (CCD) and other detectors; unshielded detectors can be affected even in the outer belt, where <1 MeV protons are present. The ionising dose contributions of trapped protons and electrons are illustrated in fig. 9, which shows dose in Si (calculated with the SHIELDOSE code [14]) as a function of shielding thickness accumulated over an 800 km

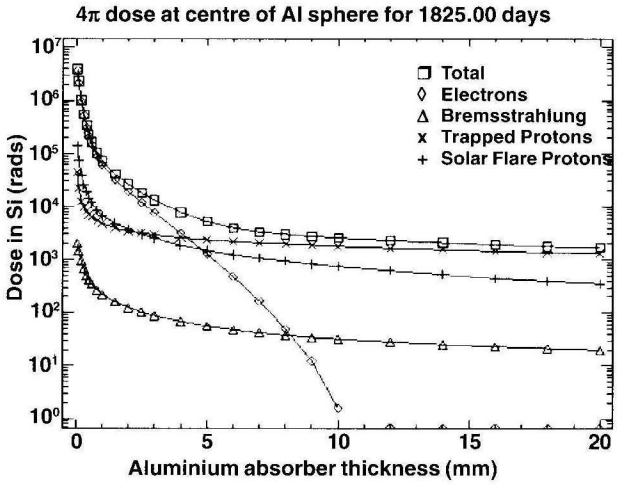

Fig. 9 Ionising doses in Si as a function of Al shielding thickness for an 800 km heliosynchronous orbit.

heliosynchronous orbit. Doses induced by solar flare protons (obtained with the JPL-91 model [15] are shown as well. Electron doses dominate for thin shieldings, while trapped and solar flare proton doses become more important for thicker shielding. It should be noted that for this orbit trapped proton doses are higher than solar flare proton doses except for the lowest shielding thicknesses.

4. Shortcomings of Present Day Radiation Belt Models

The old NASA AP-8 and AE-8 radiation belt models [6] are still the de facto standards for engineering applications. This is mainly due to the fact that up to now they are the only models that completely cover the region of the radiation belts, and have a wide energy range for both protons and electrons. It should be noted that a considerable part of the range of the NASA models was achieved by extrapolation.

The NASA models are static and are in principle only valid for the period when the data for the models were obtained [16]. In view of the dynamic characteristics of the radiation belts outlined in Section 2.4, it is clear that correspondingly dynamic models are needed for accurate predictions of mission fluxes and doses. Several efforts are under way to include dynamic behaviour in new radiation belt models, but up to now no models are available that duplicate the spatial and energy range of the NASA models. In order to achieve this, high quality data are needed from different locations in the magnetosphere, covering long time periods and with high resolution in energy, direction and time. Simple radiation monitors could easily be installed on commercial satellites, which would help the continuous upgrading needed for truly dynamic radiation belt models. However, as long as not all features of the radiation belts are fully understood or adequately modelled, high quality data are indispensable.

References

1. J.G. Roederer, *Dynamics of Geomagnetically Trapped Radiation*, Springer-Verlag, 1970.
2. M. Walt, *Introduction to Geomagnetically Trapped Radiation*, University Press, Cambridge, 1994.
3. J.F. Lemaire, D. Heynderickx and D.N. Baker (eds), "Radiation Belts. Models and Standards", *Geophysical Monograph*, **97**, AGU, 1996.
4. D.M. Sawyer and J.I. Vette, 1976, "AP-8 Trapped Proton Environment for Solar Maximum and Solar Minimum", NSSDC/WDC-A-R&S 76-06, 1976.
5. J.I. Vette, "The AE-8 Trapped Electron Model Environment", NSSDC/WDC-A-R&S 91-24, 1991.
6. J.I. Vette, "The NASA/National Space Science Data Center Trapped Radiation Environment Model Program (1964-1991)", NSSDC/WDC-A-R&S 91-29, 1991.
7. S.L. Huston, G.A. Kuck and K.A. Pfitzer, "Low Altitude Trapped Radiation Model Using TIROS/NOAA Data", in "Radiation Belts. Models and Standards", J.F. Lemaire, D. Heynderickx, and D.N. Baker (eds.), *Geophysical Monograph*, **97**, AGU, p.119, 1996.
8. A.C. Fraser-Smith, "Centered and Eccentric Geomagnetic Dipoles and Their Poles, 1600-1985", *Rev. Geophys.*, **25**, 1-16, 1987.
9. D. Heynderickx, "Comparison Between Methods to Compensate for the Secular Motion of the South Atlantic Anomaly", *Nucl. Tracks Radiat. Meas.*, **26**, 1996.
10. M.S. Gussenhoven, E.G. Mullen and D.H. Brautigam, "Improved Understanding of the Earth's Radiation Belts from the CRRES Satellite", *IEEE Trans. Nucl. Sci.*, **43**, 353-368, 1996.
11. M.S. Gussenhoven, E.G. Mullen and D.H. Brautigam, "Phillips Laboratory Space Physics Division Radiation Models", in "Radiation Belts. Models and Standards", J.F. Lemaire, D. Heynderickx, and D.N. Baker (eds.), *Geophysical Monograph*, **97**, AGU, p. 93, 1996.
12. C.E. McIlwain, "Coordinates for Mapping the Distribution of Magnetically Trapped Particles", *J. Geophys. Res.*, **66**, 3681-3691, 1961.
13. M.K. Hudson, S.R. Elkington, J.G. Lyon, V.A. Marchenko, I. Roth, M. Temerin and M.S. Gussenhoven, "MHD/Particle Simulations of Radiation Belt Formation During a Storm Sudden Commencement", in "Radiation Belts. Models and Standards", J.F. Lemaire, D. Heynderickx, and D.N. Baker (eds.), *Geophysical Monograph*, **97**, AGU, p.57, 1996.
14. S.M. Seltzer, "A Computer Code for Space Radiation Shielding Methods", NBS Technical Note 116, 1980.
15. J. Feynman, G. Spitale, J. Wang and S. Gabriel, "Interplanetary Proton Fluence Model: JPL 1991", *J. Geophys. Res.*, **98**, 13,281-13,294, 1993.
16. D. Heynderickx, J. Lemaire and E.J. Daly, "Historical Review of the Different Procedures Used to Compute the L-Parameter", *Nucl. Tracks Radiat. Meas.*, **26**, 325-331, 1996.

(Received 7 July 1999)